Ocean Engineering 149 (2018) 205–216

Contents lists available at ScienceDirect

Ocean Engineering

journal homepage: www.elsevier.com/locate/oceaneng

# Behavior of large piled-raft foundation on clay soil

Shivanand Mali *, Baleshwar Singh

*Department of Civil Engineering, Indian Institute of Technology Guwahati, Guwahati 781039, Assam, India*

ARTICLE INFO

*Keywords:*
Piled-raft
Numerical modeling
Clay soil
Settlement ratio
Bending moment ratio
Shear force ratio
Raft-soil stiffness ratio

ABSTRACT

The piled-raft foundation is usually adopted to support the offshore structures. In the present study, a large piled-raft has been simulated numerically through 3-D finite element modeling. The objective of the present study was to investigate the effect of pile spacing, pile length, pile diameter and raft-soil stiffness ratio on the settlement, load-sharing, bending moments, and shear force behavior of large piled-raft foundation. The results indicated that with increase in pile spacing up to the 5 to 6 times of the pile diameter, both average settlement ratio and differential settlement ratio decreased effectively and thereafter it increased gradually. Raft with smaller raft-soil stiffness ratio and larger pile group to raft width ratio observed to be effective in decreasing the average settlement ratio. The load-sharing ratio decreased with increase in pile spacing whereas; it increased with increase in pile length. With increase in pile spacing, bending moment ratio increased and as the length of pile increased bending moment ratio decreased up to pile group to raft width ratio of 0.6 and thereafter it increased.

## 1. Introduction

The piled-raft is a geotechnical foundation consisting of the three elements raft, piles and soil. Burland (1977) proposed that the piles can be used to reduce the settlement of the raft foundation. In piled-raft foundation, the total load of the superstructure is partly carried by the piles and the raft. The distribution of total load among the piles, raft and soil depends on their relative stiffnesses. Based on the dimensions of the raft and piles, the piled-raft has been classified as a small piled-raft ($B_r/L_p < 1$) and large piled-raft ($B_r/L_p > 1$) (Viggiani, 2001; Sanctis and Mandolini, 2006; Mandolini et al., 2013). In a small piled-raft, the flexural stiffness of the raft is usually high and the differential settlement does not represent a problem. Here, the primary reason to add the piles is to achieve a sufficient factor of safety against the bearing failure. However, in a large piled-raft, piles are added essentially to reduce the settlement.

Poulos (2001) indicated that the 3-D numerical modeling is the most reliable method for the analysis of the piled-raft foundation in a clay soils. The maximum settlement, differential settlement, raft bending moments and shear force, axial loads and pile bending moments are considered as crucial parameter for optimum design of piled-raft foundation. Several researchers have been investigated the settlement (Prakoso and Kulhawy, 2001; Cho et al., 2012; Sinha and Hanna, 2016) and bearing behavior (Reul, 2004; Sanctis and Mandolini, 2006; Lee et al., 2010) of a piled-raft foundation on clay soils by numerical modeling.

Oh et al. (2008) conducted a study on the piled-raft foundation in sandy soil by numerical modeling. They reported that with increase in raft thickness and pile spacing, the bending moment of the piled-raft increased. The different design aspects of the piled-raft foundation have been reported by Seo et al. (2003), and Reul and Randolph (2004). Ghalesari et al. (2015) suggested that the piled-raft foundation can be adopted as offshore foundation to reduce the settlement and to enhance the bearing capacity of the foundation. Furthermore, Poulos and Devdas (2005), Poulos and Bunce (2008), Poulos et al. (2011), Rabiei and Choobbasti (2016) indicated that the piled-raft can be used as an effective and economic foundation alternative for tall buildings to control the settlement and to enhance the bearing capacities.

In addition to this, Nguyen et al. (2014) conducted a parametric study of large piled-raft foundations in sandy soil through finite element modeling. They indicated that the concentrated pile arrangement method can help to considerably reduce the settlements and bending moments of the raft. However, very few parametric studies by means of numerical modeling have been reported for the large piled-raft foundation on a clay soils. Therefore, the effect of different parameters on large piled-raft foundation needs to be investigated. The intended large piled-raft foundation can be used for the construction of residential or commercial buildings situated near onshore line where mostly undrained conditions prevail.

### 1.1. Objective and scope of the study

In a large piled-raft foundation, the width of raft is relatively larger in

* Corresponding author.
*E-mail addresses:* shivanand.mali@iitg.ernet.in (S. Mali), baleshwar@iitg.ernet.in (B. Singh).

https://doi.org/10.1016/j.oceaneng.2017.12.029
Received 6 July 2017; Received in revised form 12 October 2017; Accepted 10 December 2017

comparison with the length of piles and the piles are added primarily to reduce the settlements. Thus, the present paper aims to analyze the settlement, load-sharing, bending moment and shear force behavior of large piled-raft foundation subjected to vertical load on a clay soil. In order to understand these behaviors, the influence of various parameters such as pile spacing ($S_p$), pile length ($L_p$), pile diameter ($d_p$) and raft-soil stiffness ratio ($K_{rs}$) was studied through PLAXIS 3D software. A series of numerical simulations for different piled-raft configurations was performed to fulfill the aim of the present study. Based on the parametric study, the approximate design steps and concluded observations are summarized.

## 2. Finite element modeling

### 2.1. Finite element mesh and boundary conditions

The model consisted of the soil mass with unaffected boundary conditions, foundation geometry with square raft of 45 m width ($B_r$), interface element and the applied uniformly distributed load ($q$) of 200 kPa. Fig. 1 shows the typical finite element mesh, plan view of quarter piled-raft and 10-node tetrahedral soil element with 3-node embedded beam element. The water table was considered at ground level. From the edge of the raft, lateral soil domain boundaries of the model were placed at a distance of twice the width of raft and restrained against horizontal translation but with vertical translation of soil being allowed. Fig. 2 shows the cross sectional view of piled-raft foundation. The bottom soil boundary was at a vertical distance of a twice the width of raft plus two-third the length of pile and was restricted from both horizontal and vertical translations (Gandhi and Maharaj, 1995).

Globally fine mesh has been selected for the entire soil domain and relatively very fine mesh was chosen in the vicinity of the structural elements. The very fine meshing has been generated with coarseness factor of 0.25 i.e. the size of element in very fine meshing is 0.25 times that of size of element in fine meshing. The analysis of piled-raft involved two stages, namely initial stage and loading stage. In the initial stage, the soil domain was activated and in the loading stage, the piled-raft geometry and applied load were activated and run was made. As reported by Shrestha et al. (2017), in the present study undrained soil response was modeled for the precise modeling of onshore piled-raft foundations. From the preliminary analysis of the piled-raft under the applied loading, it was found that the selected lateral boundaries of the soil domain were sufficient because the observed zone of plastic strain developed in the soil was equal to width of raft ($B_r$) laterally from the edge of the raft.

### 2.2. Constitutive modeling

Mohr-Coulomb model require lesser number of input parameter of soil. Therefore, in present study the soil was modeled as 10-node tetrahedral elements with the elastic-perfectly plastic Mohr-Coulomb model. The parameters required for modeling consisted of cohesion, angle of internal friction, Young's modulus and Poisson's ratio. As per the Mohr-Coulomb failure criteria, the yielding or failure takes place in the soil mass as the mobilized shear stress at any plane becomes equal to the shear strength of soil. To simplify the analysis process, the constant values of the material parameters were used for entire soil domain (Ranjan and Rao, 2007).

The raft and piles were modeled as 5-node triangular plate elements and 4-node line elements, respectively. The raft and piles remains in elastic state as their modulus of elasticity is greater than the soil; therefore, the material of raft and piles were considered to be linear-elastically. The piles and raft were connected by rigid connection.

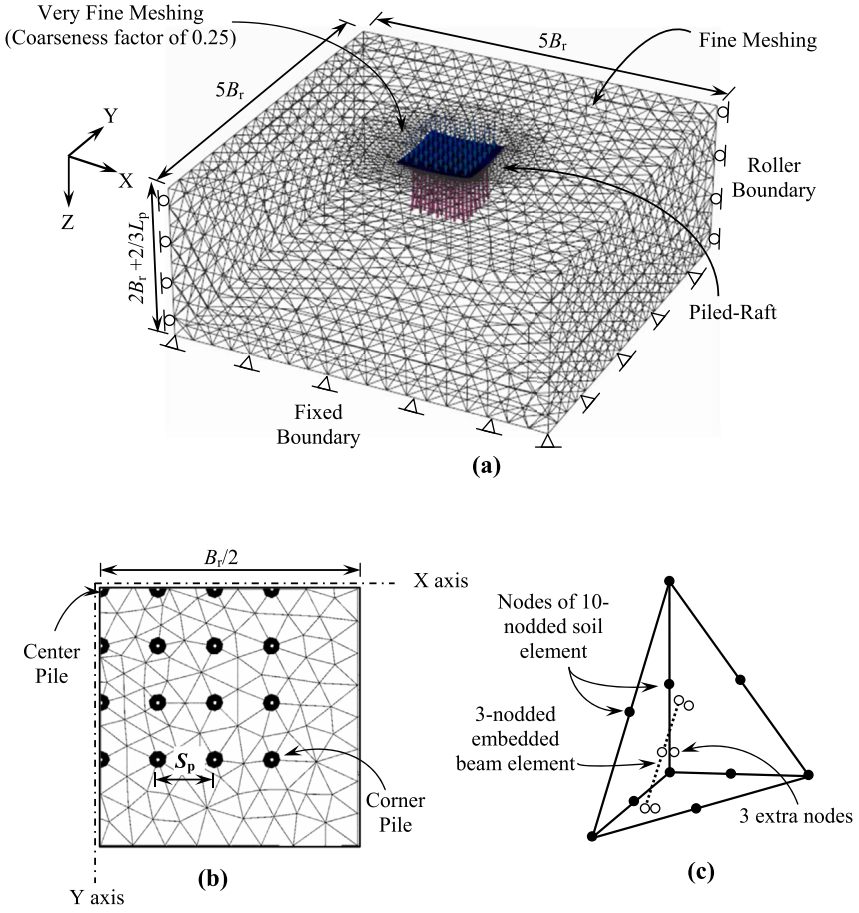


**Fig. 1.** **(a)** Typical finite element mesh used in the parametric study, **(b)** Plan view (quarter of the piled-raft) and, **(c)** 10-node tetrahedral element with 3-node embedded beam element.

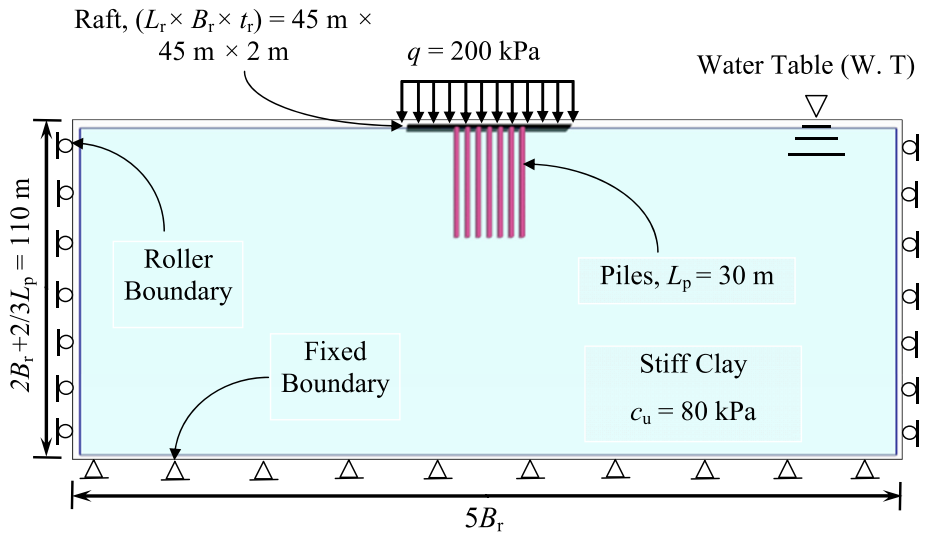


**Fig. 2.** Cross section of piled-raft foundation (For $B_g/B_r$ = 0.6, $S_p$ = 4.6 m).

Moreover, the raft-soil interface was considered as a smooth contact with strength reduction factor ($R_{inter}$) of 0.67. The $R_{inter}$ indicates the strength of interface element as a percentage of the shear strength of adjacent soil and is indicated by the Eqns. (1) and (2).

$$c_i = R_{inter} \times c_{soil} \tag{1}$$

$$tan\varnothing_i = R_{inter} \times tan\varnothing_{soil} \tag{2}$$

where $c_i$ is the interface cohesion, $\varphi_i$ is the interface friction angle, $c_{soil}$ is the surrounding soil cohesion, and $\varphi_{soil}$ is the surrounding soil friction angle.

Fig. 3 shows the pile-soil interface technique used in the present study (Jeong et al., 2004). Fig. 3(a) and (b) show the "no slip" and "slip" conditions between the soil and pile elements, respectively. The interaction between the soil and the pile was modeled by the embedded interface elements of 3-node line elements with pairs of nodes instead of single nodes. One node of each pair belongs to the beam element, whereas other node is point in the 10-node wedge element belonging to soil element.

In the finite element formulation, the coordinates of each node pair are identical, which indicates that the interface element has a zero thickness (h = 0) (Fig. 3(a)). Interface elements follow the Mohr-Coulomb failure criterion; once the shear stress (τ) in soil equal to the yield shear strength of the soil ($\sigma_h tan\varphi + c_u$), the slippage occurs at the interface (Fig. 3(b)). The elastic shear behavior exists until the shear stress reaches a critical value ($\gamma_{crit}$), beyond which the shear displacement increases without an accompanying increase in shear stress (Fig. 3(c)). After meshing, interfaces are composed of 12-node interface elements. The interface elements were introduced mainly to simulate the displacement discontinuity between the structural elements (piles) and the soil mass.

In practice, the pile installation changes the state of stress in surrounding soil. The stress change in soil is mainly governed by the pile installation process (boring or driving), pile dimensions (length and diameter) and, type and state of the soil (soft or stiff). In the earlier numerical studies, the stress change in the soil due to pile installation was neglected (Baguelin and Frank, 1982; Cho et al., 2012; Lee et al., 2010; Ghalesari et al., 2015). In the present study bored piles are used which

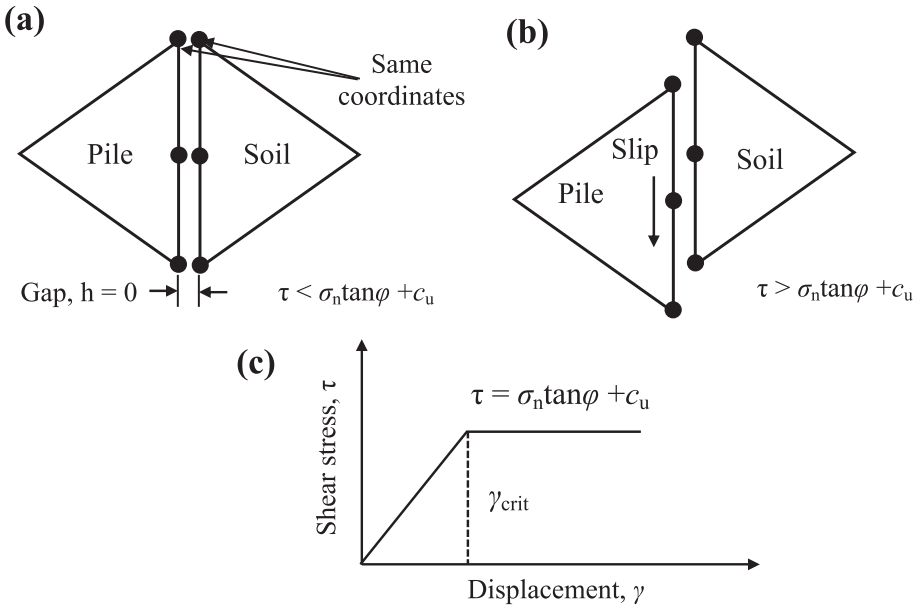


**Fig. 3.** Pile-soil interface modeling technique (a) no slip, (b) slip and (c) Coulomb frictional law (Jeong et al., 2004).

cause a limited disturbance of the surrounding soil during pile installation (Brinkgreve et al., 2015).

### 2.3. Model validation

The present finite element model in the PLAXIS 3D has been validated by comparing with the results reported by Sinha and Hanna (2016). A raft of 24 m × 24 m size with 2.0 m thickness and 16 piles of 1.0 m diameter with different lengths (5 m, 10 m and 15 m) were used in their study. The piles were spaced at six times of pile diameter and uniformly distributed load of 0.5 MPa was applied on the foundation. The material properties of the soil, raft and piles are shown in Table 1. The comparative results of the present study with the reported results are shown in Fig. 4. It can be seen that the results of the present study are in reasonably good agreement with that of reported results for the different length of piles.

## 3. Parametric study

In this section, the settlement, load-sharing, bending moment and shear force behavior of the large piled-raft foundation is studied with the variation of $S_p$, $L_p$, $d_p$ and $K_{rs}$. The properties of soil, raft and pile are summarized in Table 2. The geometrical dimensions of piled-raft and the values of $E_s$, $E_r$, $K_{rs}$, $E_p$ have been selected from Viggiani (2001). Fig. 5 shows the different pile arrangements for the parametric study. The layout of piles beneath the raft for different pile spacings are shown in Fig. 6. Vertical settlement profile of the raft is as shown in Fig. 7 (see Table 3).

**Table 1**
Material properties used in the validation (Sinha and Hanna, 2016).

| Material | Properties | Unit | Value |
|---|---|---|---|
| Soil | Young's modulus, $E_s$ | MPa | 54 |
| | Poisson's ratio, $\nu_s$ | – | 0.15 |
| | Unit weight, $\gamma$ | kPa | 19 |
| | Angle of internal friction, $\varphi$ | ° | 20 |
| Raft | Young's modulus, $E_r$ | GPa | 34 |
| Pile | Young's modulus, $E_p$ | GPa | 25 |
| | Poisson's ratio, $\nu_p$ | – | 0.2 |

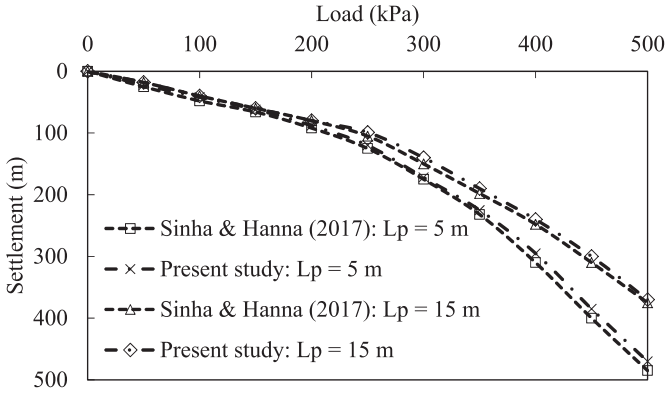


**Fig. 4.** Comparison of load settlement behavior of present study with the results of Sinha and Hanna (2016).

**Table 2**
Material properties used in the parametric analysis.

| Material | Properties | Unit | Value |
|---|---|---|---|
| Soil | Unsaturated unit weight, $\gamma_{unsat}$ | kN/m$^3$ | 16 |
| | Young's modulus, $E_s$ | MPa | 25 |
| | Poisson's ratio, $\nu_s$ | – | 0.495 |
| | Angle of internal friction, $\varphi$ | ° | 0 |
| | Undrained cohesion | kPa | 80 |
| | Adhesion factor, $\alpha$ | – | 0.55 |
| Raft | Young's modulus, $E_r$ | GPa | 25 |
| Pile | Young's modulus, $E_p$ | GPa | 25 |
| | Poisson's ratio, $\nu_p$ | – | 0.25 |

**Table 3**
Geometric configurations of piled-raft model for parametric analysis.

| Parameters | Unit | Value |
|---|---|---|
| Raft width, $B_r$ | m | 45[a] |
| Raft width, $L_r$ | m | 45[a] |
| Raft thickness, $t_r$ | m | 1, 2[a], 3 |
| Corresponding raft-soil stiffness ratio, $K_{rs}$ | – | 0.01, 0.09[a], 0.31 |
| Piled group to raft width ratio, $B_g/B_r$ | – | 0.2, 0.4, 0.6[a], 0.8 |
| Pile length, $L_p$ | m | 10, 20, 30[a] |
| Pile spacing, $S_p$ | m | 4.5[a] - 36 |
| Pile diameter, $d_p$ | m | 0.5, 1.0[a], 1.5, 2.0 |

[a] Indicates standard value if not varied.

The results are plotted in the form of average settlement ratio ($R_{avg}$), differential settlement ratio ($R_{diff}$), load-sharing ratio ($G_{PR}$), bending moment ratio ($R_{BM}$) and shear force ratio ($R_{SF}$). The $R_{avg}$ is defined as the ratio of average settlement of piled-raft to the average settlement of unpiled-raft. The average settlement ($W_{avg}$) and differential settlement ($W_{diff}$) are expressed in Eqns. (3) and (4). The $R_{avg}$ and $R_{diff}$ and are represented by Eqns. (5) and (6). The $G_{PR}$ is defined as the ratio of total load carried by the piles ($R_{pile}$) to the total applied load (static load) ($R_{total}$) on the foundation. The objective of introducing $G_{PR}$ is to know the percentage load carried by piles and raft, separately. $R_{pile}$ is calculated by summing the axial load carried by the individual piles at its head.

Eqn. (7) indicates the expression for $G_{PR}$. The value of 1.0 for $G_{PR}$, indicates a freestanding pile group, and value of 0 for $G_{PR}$, describes an unpiled-raft; whereas, $G_{PR}$ in the range of 0–1 indicates the piled-raft foundation. $R_{BM}$ and $R_{SF}$ are the ratios of maximum bending moment of piled-raft to the maximum bending moment of unpiled-raft and maximum shear force of piled-raft to the maximum shear force of unpiled-raft, respectively. The raft-soil stiffness ratio ($K_{rs}$) for different raft thicknesses is calculated from Eqn. (8) which has been given by Fraser and Wardle (1976).where $E_r$, is the modulus of elasticity of the raft, $\nu_r$ is the raft Poisson's ratio, $E_s$ *is* the modulus of elasticity of the soil, $\nu_s$ is the soil Poisson's ratio, $t_r$ is the raft thickness and $B_r$ is the raft width.

$$W_{avg} = \frac{1}{3}(2w_{center} + w_{corner}) \tag{3}$$

$$W_{diff} = w_{center} - w_{corner} \tag{4}$$

$$R_{avg} = \frac{W_{avg}\ of\ piled-raft}{W_{avg}\ of\ unpiled-raft} \tag{5}$$

$$R_{diff} = \frac{Diff.settlement\ of\ piled-raft}{Diff.\ settlement\ of\ unpiled-raft} \tag{6}$$

$$G_{PR} = \frac{R_{pile}}{R_{total}} \tag{7}$$

$$K_{rs} = \frac{4 \times E_r \times (1-\nu_s^2)}{3 \times E_s(1-\nu_r^2)} \times \frac{t_r^3}{B_r^3} \tag{8}$$

### 3.1. Effect of pile spacing ($S_p$)

A square (45 m × 45 m) raft with $K_{rs}$ of 0.09 and piles of $L_p/d_p$ equal to 30 and $d_p$ of 1.0 m was analyzed for different $B_g/B_r$ ratios (0.2, 0.4, 0.6, and 0.8). The effects of $S_p/d_p$ for different $B_g/B_r$ ratios on $R_{avg}$ and $R_{diff}$ are shown in Fig. 8a and b, respectively. $R_{avg}$ corresponds to 1.0 indicates that the average settlement of the piled-raft is equal to the average settlement of the unpiled-raft.

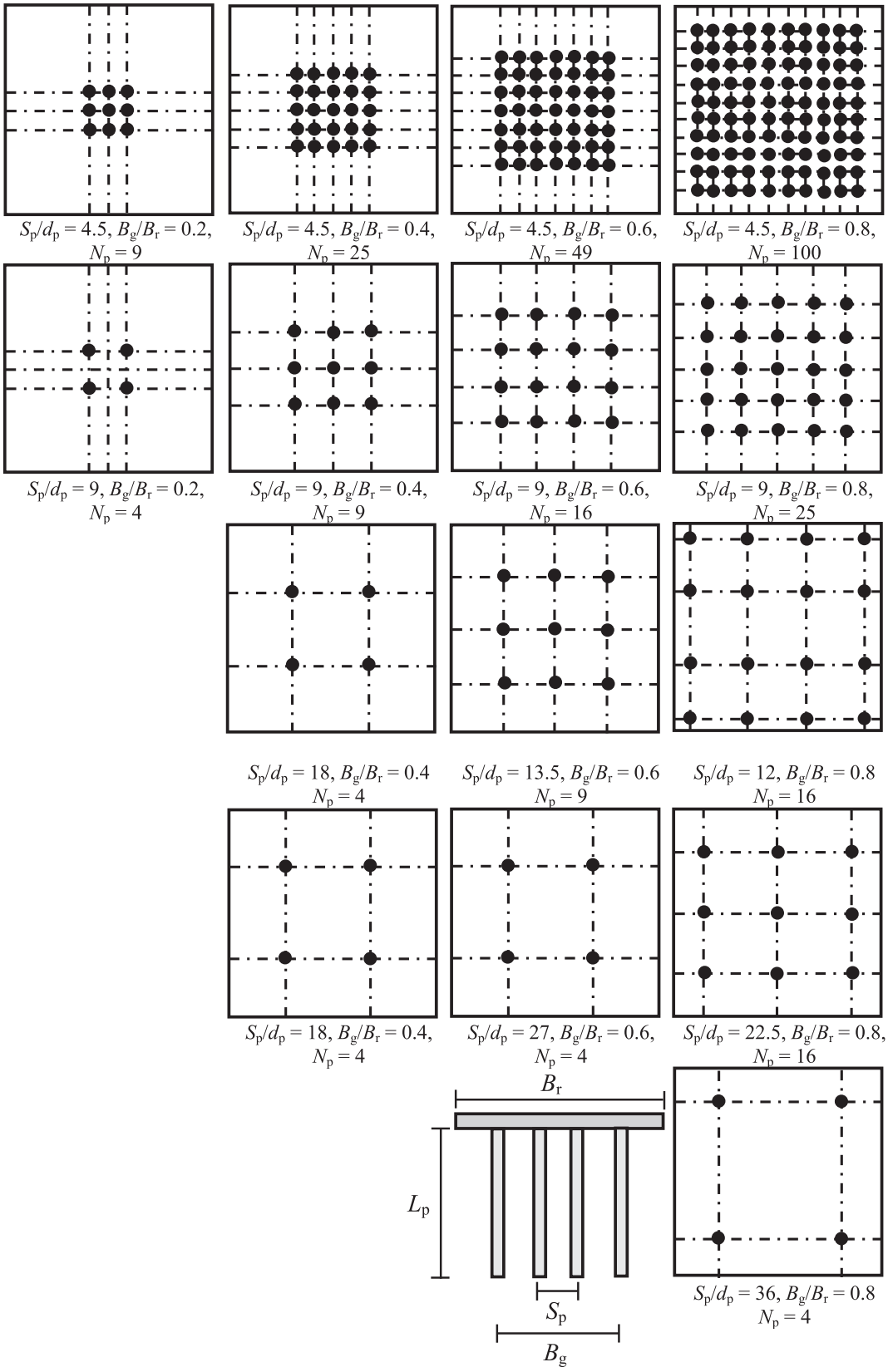


**Fig. 5.** Pile arrangements for parametric study.

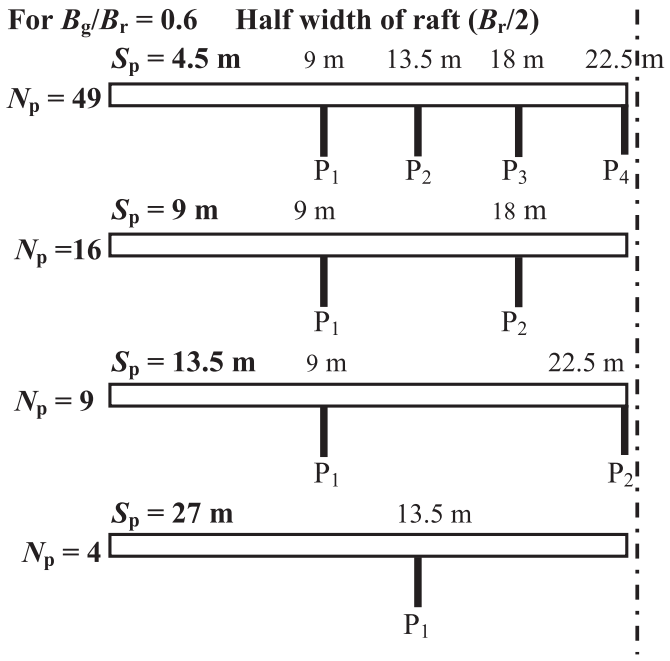


**Fig. 6.** Half layout of piles in the piled-raft for different pile spacings.

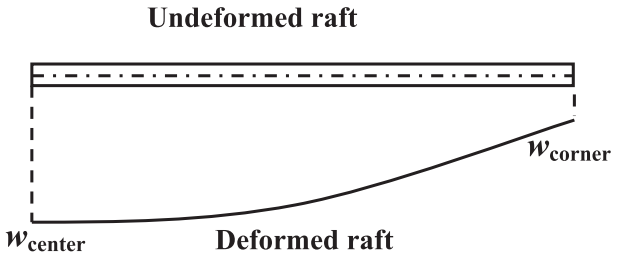


**Fig. 7.** Definition of raft settlement.

It can be seen that with increase in $S_p/d_p$ from zero, $R_{avg}$ decreases for different $B_g/B_r$ ratios and the decrease is noted to be more for higher $B_g/B_r$ ratio of 0.8 (Fig. 8(a)). For any $B_g/B_r$ ratio the $R_{avg}$ attains a minimum value at $S_p/d_p$ = 5–6 (approx.) and then afterword it increases gradually. Beyond $S_p/d_p$ of 5–6, the number of piles decreases and also a group of piles might have started to behave as individual pile elements. Thus, from the average settlement point of view, the $S_p/d_p$ of 5–6 can be considered as optimum value.

As the $S_p/d_p$ increases, $R_{diff}$ decreases for different $B_g/B_r$ ratios and the decrease is noted to be more for lower $B_g/B_r$ ratio of 0.2 (Fig. 8(b)). $R_{diff}$ corresponds to 1.0 indicates that the differential settlement of the piled-raft is equal to the differential settlement of the unpiled-raft. At any $B_g/B_r$ ratio, $R_{diff}$ decreases initially up to $S_p/d_p$ = 6 (approx.) and subsequently increases. At $B_g/B_r$ ratios of 0.2 piles are mostly concentrated near the central portion of the raft due to which $R_{diff}$ decreases. For minimizing the differential settlement, pile should be placed near the central portion of the raft with $S_p/d_p$ of 5–6.

Fig. 9 shows the Effect of pile spacing on average settlement ratio for different raft-soil stiffnesses and $B_g/B_r$ ratios. It can be observed that for same $S_p/d_p$ and $B_g/B_r$ ratio, with increase in raft-soil stiffness ratio ($K_{rs}$), $R_{avg}$ increases. For same $K_{rs}$, with increase in $B_g/B_r$ ratio, $R_{avg}$ is observed to be decreases. Therefore, raft with smaller $K_{rs}$ and larger $B_g/B_r$ ratio can be selected to decrease the $R_{avg}$ effectively. Fig. 10 shows the load-settlement plot for piled-raft (*PR*), pile group (*PG*), unpiled-raft (*UR*), raft in piled-raft ($R_{pr}$), and piles in piled-raft ($G_{pr}$). It can be seen that the load carried by *PG* and *UR* is higher than that of $G_{pr}$ and $R_{pr}$, respectively. Such behavior may be due to the interaction of piles and raft in piled-raft.

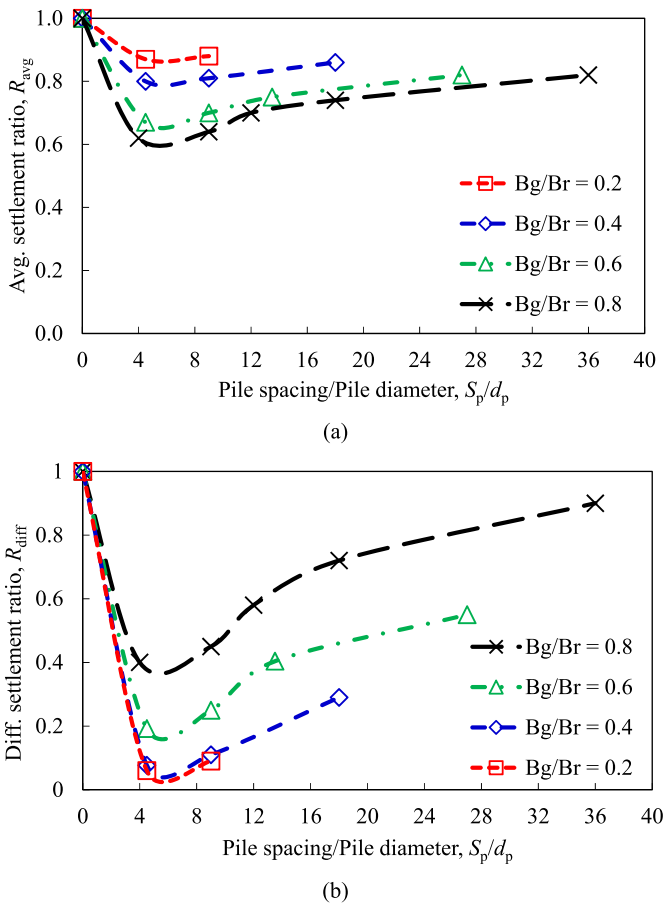


**Fig. 8.** Effect of pile spacing on (a) average settlement ratio and (b) differential settlement ratio.

At any settlement value the load carried by *PR* is equal to the load carried by $R_{pr}$ and $G_{pr}$.

Fig. 11 shows the effect of $S_p/d_p$ on $G_{PR}$ for different $B_g/B_r$ ratios. $G_{PR}$ of 1.0 indicates that the total load of the superstructure is carried by the piles only. It can be seen that as the $S_p/d_p$ increases from 4 to 36, $G_{PR}$ decreases linearly. Since, with increase in $S_p/d_p$, the number of piles decreases; consequently, the contact pressure beneath the raft increases.

The effect of $S_p/d_p$ on $R_{BM}$ and $R_{SF}$ for different $B_g/B_r$ ratios is shown in Fig. 12(a) and (b), respectively. At any $B_g/B_r$ ratio, with increase in $S_p/d_p$, $R_{BM}$ decreases initially up to $S_p/d_p$ = 5 (approx.) and thereafter it increases (Fig. 12(a)). At same $S_p/d_p$, $R_{BM}$ is observed to be less for lower $B_g/B_r$ ratio. Like differential settlement, for bending moment, pile should be placed near the central portion of the raft with lower $S_p/d_p$ ratio. For any $B_g/B_r$ ratios, with increase in $S_p/d_p$, $R_{SF}$ increases gradually. At same $S_p/d_p$, $R_{SF}$ is observed to be lesser for higher $B_g/B_r$ ratio (Fig. 12(b)). (see Fig. 14)

### 3.2. Effect of pile length ($L_p$)

In order to understand the effect $L_p$, simulations were carried on a piled-raft with $L_p/d_p$ of 10, 20 and 30, and piles were spaced at $S_p = 5d_p$. Fig. 13(a) and (b) show the effect of $L_p/d_p$ on $R_{avg}$ and $R_{diff}$ for different $B_g/B_r$ ratios. The results show that $R_{avg}$ decreases with increase in $L_p/d_p$ for every $B_g/B_r$ ratios. The decrease in settlement is attributed to the increase in the amount of skin friction with increase in $L_p/d_p$. In addition to this, the decrease of $R_{avg}$ observed to be more for larger $B_g/B_r$ ratio of 0.8 (Fig. 13(a)). Therefore, to minimize $R_{avg}$, the more numbers of piles with longer lengths are the most effective. In comparison with the $R_{avg}$, the trends of decrease in $R_{diff}$ for different $B_g/B_r$ ratio are dissimilar

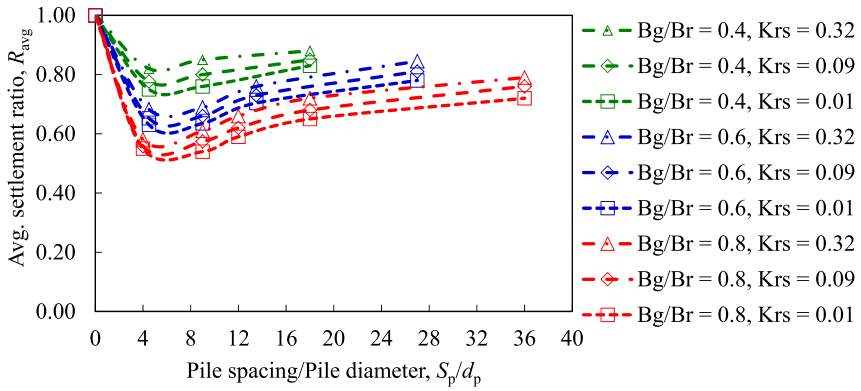


**Fig. 9.** Effect of pile spacing on average settlement ratio for different raft-soil stiffnesses and $B_g/B_r$ ratios.

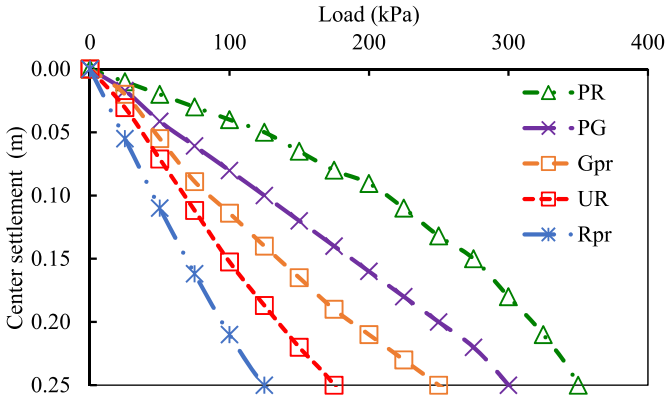


**Fig. 10.** Load-settlement relationship for the piled raft (*PR*), pile group (*PG*), unpiled-raft (*UR*), pile group in piled raft ($G_{pr}$) and raft in piled-raft ($R_{pr}$).

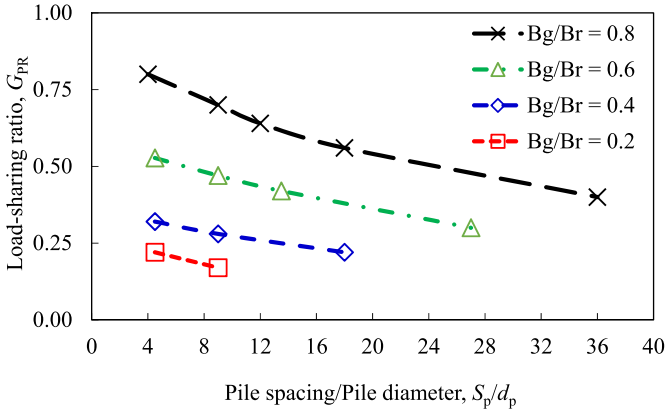


**Fig. 11.** Effect of pile spacing on load-sharing ratio and for different $B_g/B_r$ ratios.

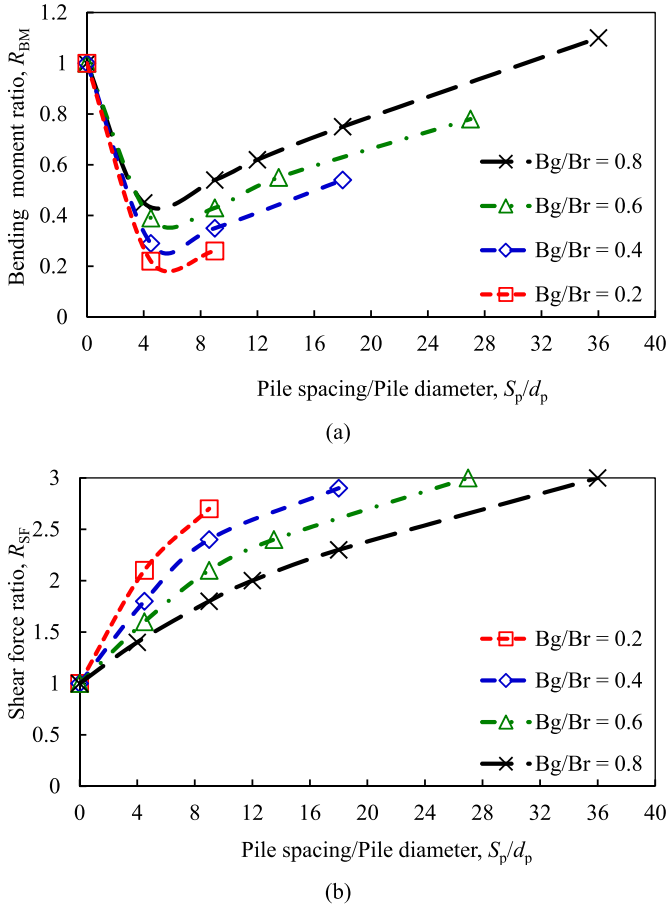


**Fig. 12.** Effect of pile spacing and $B_g/B_r$ on (a) bending moment ratio and (b) shear force ratio.

(Fig. 13(b)). $R_{diff}$ decreases with increase in $L_p/d_p$ for $B_g/B_r$ ratio of 0.2 and 0.6, then it increases for $B_g/B_r = 0.8$. Fig. 13 presents the effect of $L_p/d_p$ on $G_{PR}$ for different $B_g/B_r$ ratios. As expected, the $G_{PR}$ increases linearly as the $L_p/d_p$ increases and the increase is more at higher $L_p/d_p$. Fig. 15 shows the combined effect of effect of $L_p/d_p$ and $B_g/B_r$ ratios on $R_{BM}$ and $R_{FM}$. With increase in $B_g/B_r$ ratios, $R_{BM}$ decreases initially up to $B_g/B_r = 0.6$ and thereafter increases for every $L_p/d_p$ (Fig. 15(a)). Thus, for minimum $R_{BM}$, higher $L_p/d_p$ can be selected. With increase in $B_g/B_r$, $R_{SF}$ increased gradually for all $L_p/d_p$ (Fig. 15(b)). Thus, for minimum $R_{SF}$, it can be suggested to select lower $L_p/d_p$.

### 3.3. Effect of pile diameter ($d_p$)

In order to understand the effect of $d_p$, simulations were conducted on a piled-raft with varying $d_p$ from 0.5 to 2.0 m. It can be observed that $R_{avg}$ decreases as the $d_p$ increases (Fig. 16(a)). An increase in $d_p$ (up to 1.0 m for $B_g/B_r = 0.6$ and 0.8) might attributed the increased stiffness of the pile-raft. At $d_p$ equal to 1.0 m, the piled-raft system might have achieved the maximum stiffness. The effect of $d_p$ on $R_{diff}$ is plotted in Fig. 16(b). As the $B_g/B_r$ ratio changes from 0.2 to 0.6, the $R_{diff}$ decreases up to $d_p = 1.0$ m and it remains constant thereafter. As the $B_g/B_r$ ratio changes from 0.6 to 0.8, $R_{diff}$ increases significantly for every pile diameter.

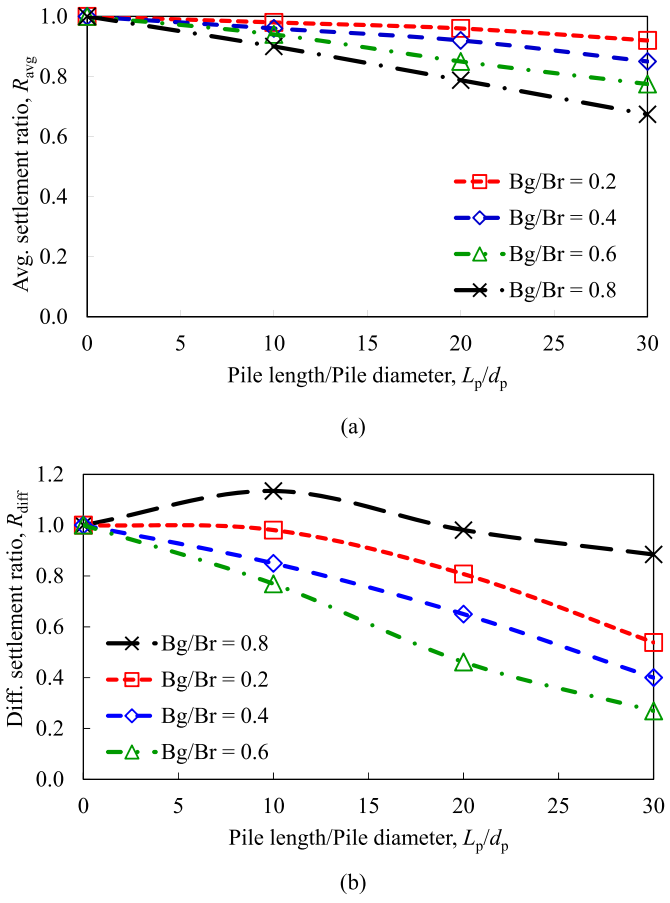


**Fig. 13.** Effect of pile length on (a) average settlement ratio and (b) differential settlement ratio.

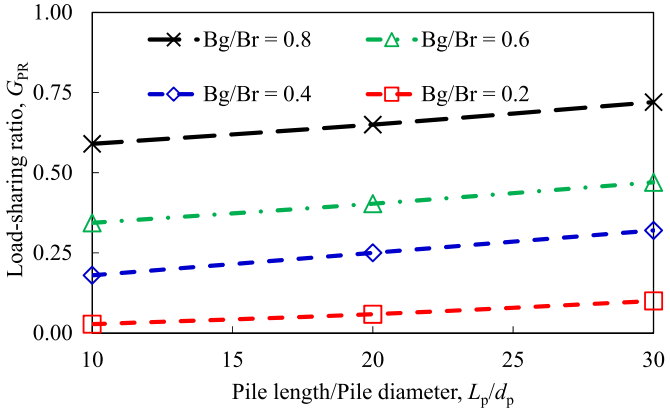


**Fig. 14.** Effect of pile length on load-sharing ratio.

Fig. 17 shows the variation of $G_{PR}$ with $d_p$ for different $B_g/B_r$ ratios. With increase in $d_p$, $G_{PR}$ increases and the increase is noted to be marginal beyond $d_p$ of 1.0 m for every $B_g/B_r$ ratios.

Fig. 18 shows the combined effect of $d_p$ and $B_g/B_r$ ratios on $R_{BM}$ and $R_{FM}$. $R_{BM}$ decreases as the $B_g/B_r$ decreases up to 0.6, and thereafter it increases. Also it can be seen that $R_{BM}$ was higher at $d_p = 4.0$ and lower at $d_p = 1.0$ (Fig. 18(a)). Fig. 18(b) shows the variation of $R_{SF}$ with $d_p$ for different $B_g/B_r$ ratios. With increase in $B_g/B_r$, for every $d_p$, $R_{SF}$ increases up to $B_g/B_r = 0.2$ and decreases thereafter. Thus, for minimum $R_{SF}$, lesser $d_p$ with higher $B_g/B_r$ ratio can be selected.

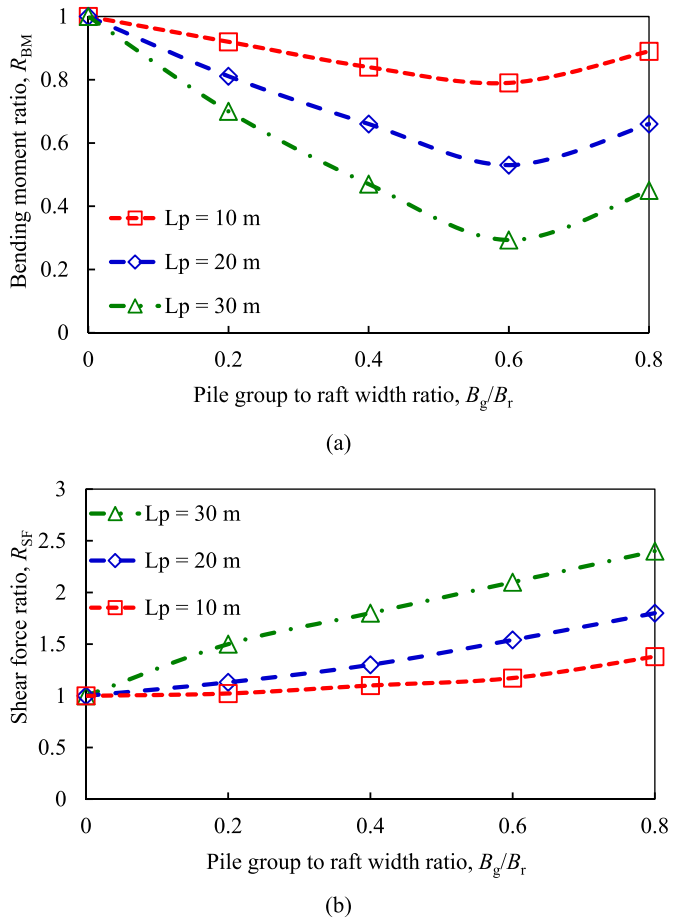


**Fig. 15.** Effect of pile length and $B_g/B_r$ on (a) bending moment ratio and (b) shear force ratio.

### 3.4. Effect of raft-soil stiffness ratio ($K_{rs}$)

In this series, simulations were carried on a piled-raft by varying $K_{rs}$ from 0.01 to 0.32 $K_{rs}$ have been varied by varying the thickness of the raft from 1 to 3 m. Fig. 19(a) and (b) shows the bending moment and shear force variation along the entire width of raft for different $K_{rs}$ at $B_g/B_r = 0.6$. It was noted that in unpiled-raft and piled-raft, the bending moment was maximum at the center of the raft (except $K_{rs} = 0.01$) and it decreases to zero at the edge of raft (Fig. 19(a)). For same raft-soil stiffness ratio ($K_{rs} = 0.09$), the bending moment response of piled-raft is dissimilar as that of unpiled-raft. From 22.5 m to 9 m span of the raft, bending moment decreases and from 9 m to 3 m span it increases and again it decreases towards the left edge of the raft.

The shear force is minimum at the center of the raft (22.5 m) and it attains maximum values at 12 m, 6 m and 0 m (Fig. 19(b)). The piles are located at a distance of 9 m, 13.5 m, 18 m and 22.5 m (Fig. 6). In general, at any $K_{rs}$ the shear force changes its sign in the vicinity of the edge pile. Fig. 20(a) shows the combined effect of $K_{rs}$ and $B_g/B_r$ on maximum bending moment ($M_{max}$) of raft and maximum shear force ($\tau_{max}$) of raft. With increase in $B_g/B_r$, $M_{max}$ decreases initially up to $B_g/B_r$ of 0.6 and after that increases for every $K_{rs}$ values. With variation of $B_g/B_r$ ratio for different $K_{rs}$ values, similar trends are observed for $\tau_{max}$ (Fig. 20(b)).

### 3.5. Behavior of piles in piled-raft

In order understand the behavior of piles in piled-raft, simulations were carried on the piled-raft with $L_p/d_p = 40$ for different $B_g/B_r$ ratios of 0.2, 0.6 and 0.8. Middle pile, edge pile and corner piles are abbreviated as

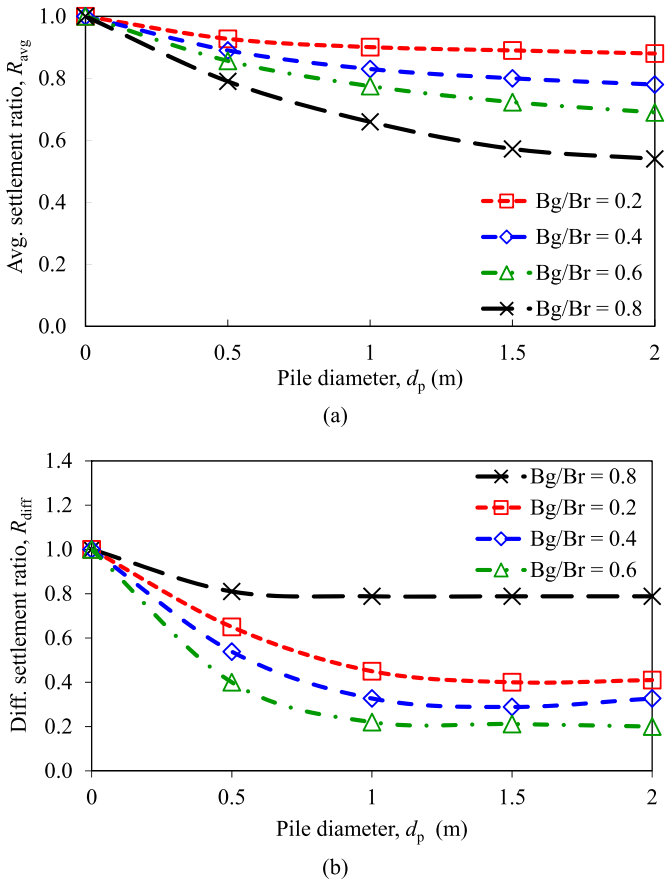


**Fig. 16.** Effect of pile diameter on (a) average settlement ratio and (b) differential settlement ratio.

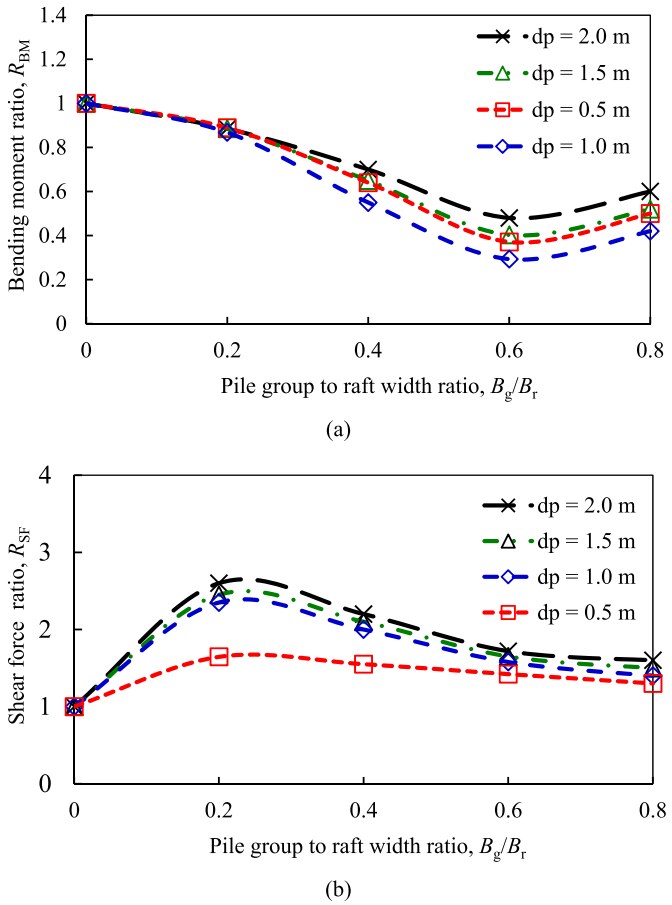


**Fig. 18.** Effect of pile diameter and $B_g/B_r$ ratios on (a) bending moment ratio and (b) shear force ratio.

MP, EP and CP, respectively. The pile abbreviated as MP_0.6, indicates the middle pile with $B_g/B_r$ ratio of 0.6. Fig. 21 shows the variation of vertical settlement and lateral displacement along the depth of piles. It can be seen that vertical settlement of piles is more at the head of the pile and it decreases nominally towards the tip of the pile (Fig. 21(a)). The vertical settlement is observed to be more in CP_0.2 and is less in CP_1.0. The settlement in corner pile is observed to be more for $B_g/B_r$ ratios of 0.2, because of lesser number of piles.

It can also be seen that of the piles are displaced laterally at its tip and the lateral displacement of pile is observed to be more in EP_1.0 (Fig. 21(b)). For smaller $B_g/B_r$ ratios, the lateral displacement of pile is noted to be lesser than that of larger $B_g/B_r$ ratio. At lower $B_g/B_r$ ratio, piles in piled-raft may possess greater soil confinement. Variation of axial force along the depth of piles is shown in Fig. 22. The axial force in the pile is observed to be higher at the head of pile and decreases towards the tip of the piles. The axial force in CP_0.2 is observed to be higher and MP_1.0 carried lesser axial force. For smaller $B_g/B_r$ ratio, the axial forces in the piles are noted to be higher than as that of larger $B_g/B_r$ ratios.

The distribution of bending moment along the depth of piles is shown in Fig. 23(a). It can be seen that the bending moment is observed to be more at the head of piles and decreases to zero at the tip of the piles. The

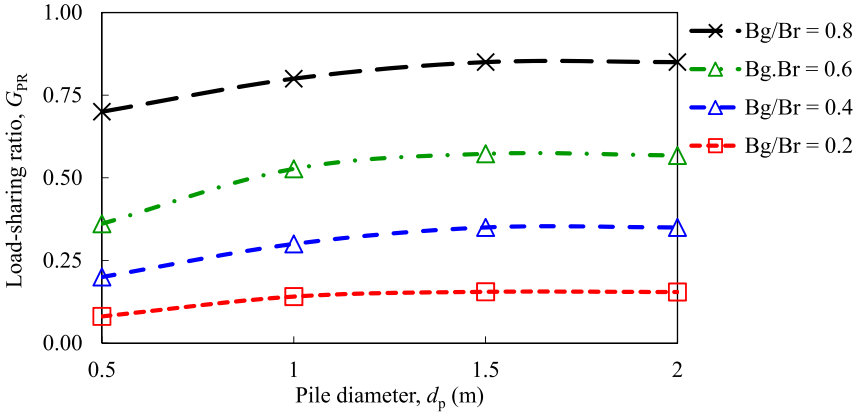


**Fig. 17.** Effect of pile diameter on load-sharing ratio.

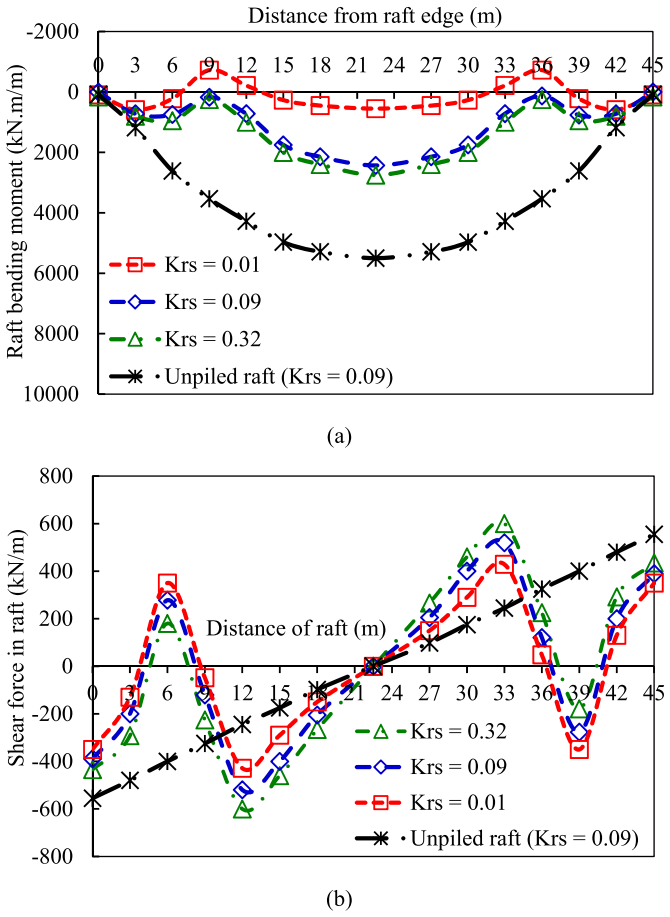


**Fig. 19.** Effect of raft-soil stiffness ratio on (a) bending moment and (b) shear force along the width of the raft ($N_p$ = 49, $S_p$ = 4.5 m, $B_g/B_r$ = 0.6).

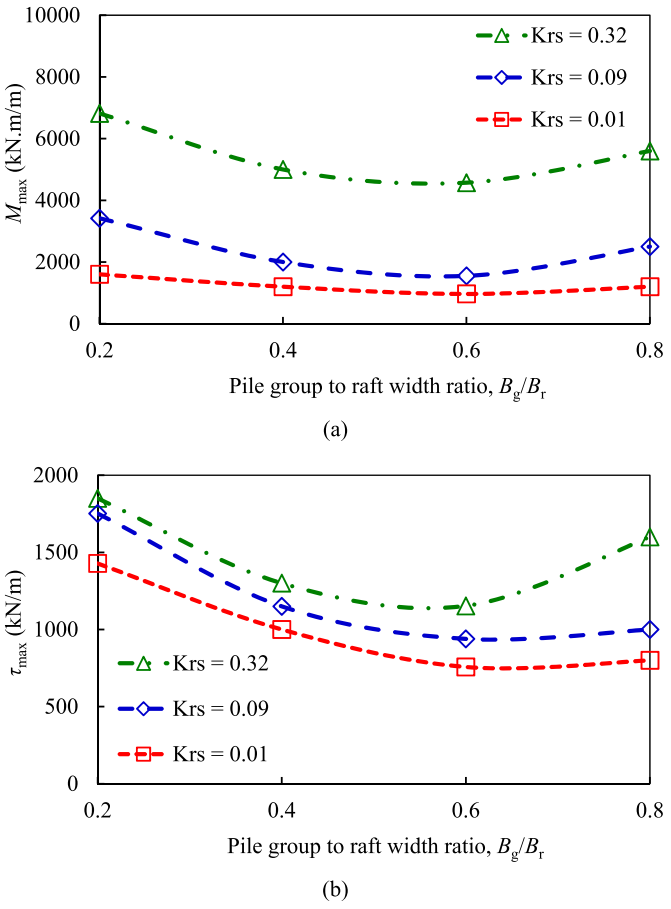


**Fig. 20.** Effect of raft-soil stiffness ratio and $B_g/B_r$ ratios on (a) maximum bending moment and (b) maximum shear force of raft.

bending moment in pile might be induced due to the lateral movement of the soil. The EP_1.0 carried higher bending moment followed by CP_0.8. Fig. 23(b) shows the distribution of shear force along the depth of piles. Shear force in the piles were observed to be higher at the head and decreased to zero (approx.) at the tip of the piles. Likewise, bending moment, the shear force in EP_0.8 was observed to be more.

## 4. Conclusions

A series of 3-D numerical analysis were carried out on a large piled-raft foundation in a clay soil under the action vertical loading. The effect of pile spacing ($S_p$), pile length ($L_p$), pile diameter ($d_p$) and raft-soil stiffness ratio ($K_{rs}$) on the settlement, load-sharing, bending moment and shear force behavior of the large piled-raft foundation were investigated. Based on the results of the present study, the following conclusions are drawn.

1. For any pile group to raft width ratio, with increase in pile spacing to diameter ratio, average settlement ratio, differential settlement ratio, and bending moment ratio decreases up to the pile spacing of 5–6 times the pile diameter and then increases. Also, load-sharing ratio decreases and shear force ratio increases. Raft with smaller raft-soil stiffness ratio and larger pile group to raft width ratio observed to be effective in decreasing the average settlement ratio. Raft and pile group in piled-raft has carried fewer loads as that of unpiled raft and free standing pile groups.
2. For any pile group to raft width ratio, with increase in pile length to diameter ratio, average settlement ratio, differential settlement ratio decreases and load-sharing ratio increase. Also, the bending moment ratio decreases up to $B_g/B_r$ = 0.6 and thereafter it increases, whereas shear force ratio increases linearly.
3. With increase in pile diameter, average settlement ratio and differential settlement ratio decreases and load-sharing ratio increases (up to pile diameter 1.0). For any pile group to raft width ratio, with increase in pile diameter from 0.5 to 1.0 m, the bending moment ratio decreases and increases thereafter. For any pile diameter, the shear force ratio increases up to pile group to raft width ratio of 0.2 and then it decreases.
4. In unpiled-raft and piled-raft, maximum bending moment and minimum shear force is obtained at the center of the raft. The bending moment was affected marginally when raft-soil stiffness increases more than 0.09. The shear force increase as the raft-soil stiffness ratio increase. At any raft-soil stiffness ratio, shear force at the edge pile is noted to be minimal as compared to inside piles. Also, shear force changes its sign in the vicinity of edge pile. As the raft-soil stiffness ratio increases, the maximum bending moment and maximum shear force in the raft increases.
5. The vertical settlement of piles is more at its head and less at its tip, whereas the lateral displacement in piles is more at its tip. Corner pile with pile group to raft width ratio of 0.2, settle more and the lateral displacement is more in pile group to raft width ratio of 0.8. The axial force, bending moment and shear force in piles are more at its head and less at its tip. Axial force is more in corner pile with pile group to raft width ratio of 0.2 and is lesser in middle pile with pile group to raft width ratio 1.0. Edge pile with pile group to raft width ratio of 0.8 carries higher bending moment and shear force.

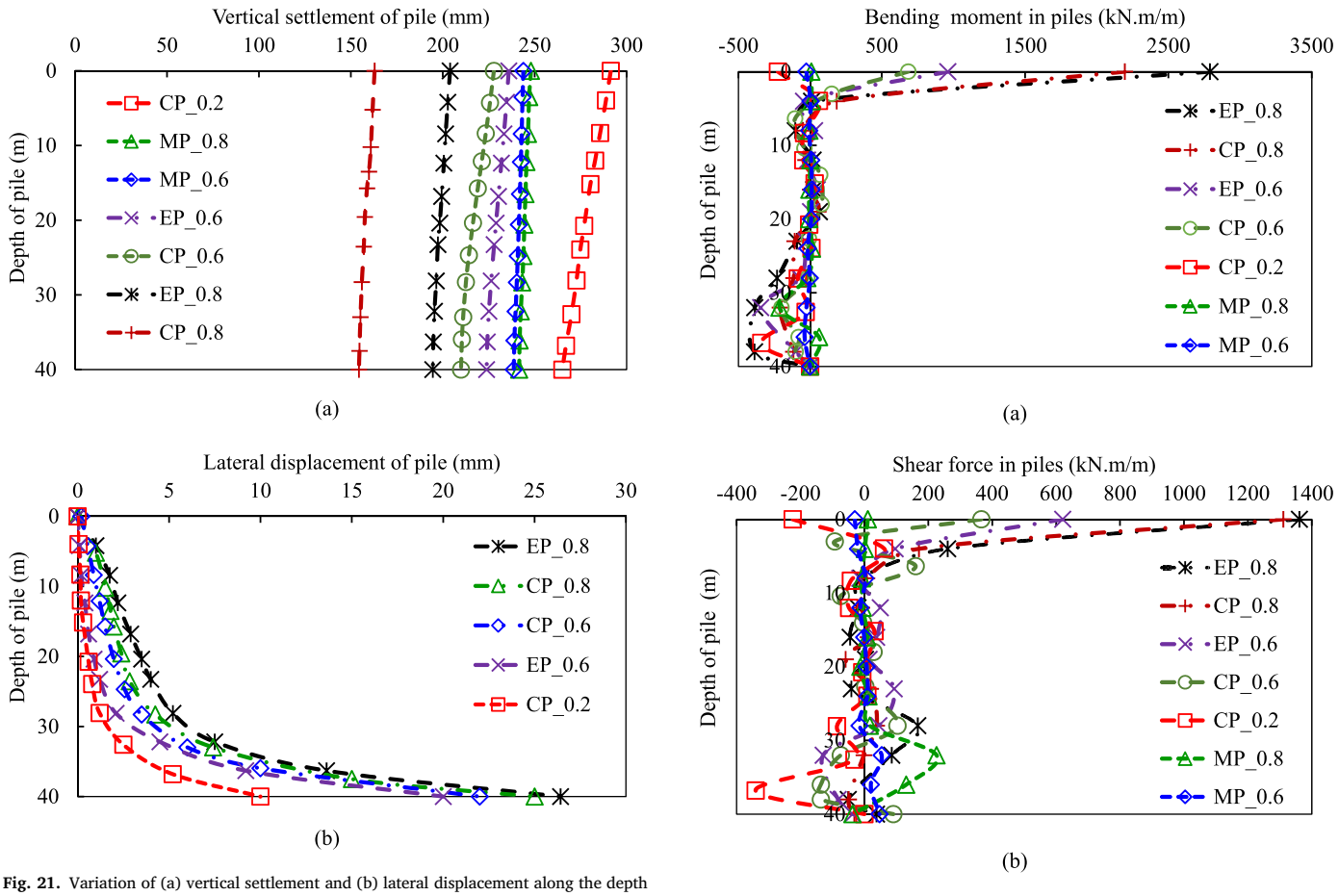


**Fig. 21.** Variation of (a) vertical settlement and (b) lateral displacement along the depth of piles.

**Fig. 23.** Variation of (a) bending moment and (b) shear force along the depth of piles.

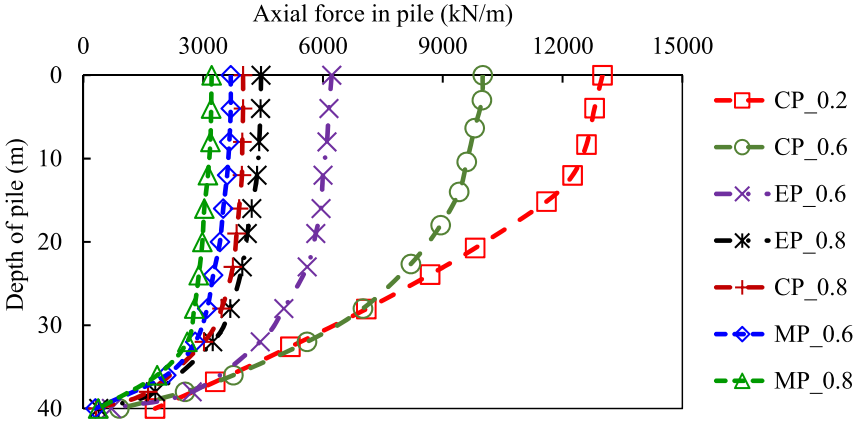


**Fig. 22.** Variation of axial force along the depth of piles.

## References


Baguelin, F., Frank, R., 1982. Theoretical Studies of Piles Using the Finite Element Method, Foundation Engineering. Georges Pilot. Presses Ponts et Chaussées.

Brinkgreve, R., Swolfs, W., Engin, E., 2015. PLAXIS User's Manual. Balkema, Rotterdam, The Netherlands, version 6.1. .

Burland, J., 1977. Piles as settlement reducers. In: Proc., 19th National Italian Geotechnical Conference Padova, Italy, vol. 2, pp. 21–34.

Cho, J., Lee, J., Jeong, S., Lee, J., 2012. The settlement behavior of piled raft in clay soils. Ocean Eng. 153–163.

Fraser, R.A., Wardle, L.J., 1976. Numerical analysis of rectangular rafts on layered foundations. Geotechnique 26 (4), 613–630.

Gandhi, S.R., Maharaj, D.K., 1995. Behavior of piled raft under uniform loading. In: Proc. Indian Geotechnical Conference (IGC-95), Bangalore, vol. 1, pp. 169–172.

Ghalesari, A.T., Barari, A.P., Fardad Amini Ibsen, L.B., 2015. Development of optimum design from static response of pile-raft interaction. J. Mater. Sci. Technol. 20, 331–343.

Jeong, S., Lee, J., Lee, C.J., 2004. Slip effect at the pile-soil interface on dragload. Comput. Geotech. 31 (2), 115–126.

Lee, J., Kim, Y., Jeong, S., 2010. Three dimensional analysis of bearing behavoir of piled raft on soft clay. Comput. Geotech. 37, 103–114.

Mandolini, A., Di Laora, R., Mascarucci, Y., 2013. Rational design of piled raft. Procedia Engineering 57, 45–52.

Nguyen, D.D.C., Kim, D.S., Jo, S.B., 2014. Parametric study for optimal design of large piled raft foundations on sand. Comput. Geotech. 55, 14–26.

Oh, E.Y.N., Huang, C., Surarak, C., Adamec, R., Balasurbamaniam, A.S., 2008. Finite element modeling for piled raft foundation in sand. In: 11th East Asia-Pacific Conference on Structural Engineering and Construction, Taiwan, pp. 19–21.

Poulos, H.G., 2001. Methods of Analysis of Piled Raft Foundations. A Report Prepared on Behalf of Technical Committee TC18 on Piled Foundations.

Poulos, H.G., Bunce, G., 2008. Foundation design for the Burj Dubai: the world tallest building. In: Proc.,The Sixth International Conference on Case Histories in Geotechnical Engineering, Arlinton, VA, pp. 11–16.

Poulos, H.G., Devdas, A.J., 2005. Foundation design for the Emirates twin towers. Dubai. Candian Geotech. J. 42, 716–730.
Poulos, H.G., Small, J.C., Chow, H., 2011. Piled raft foundation for tall buildings. Geotech. Eng. J. SEAGS AGSSEA 42 (2), 78–84.
Prakoso, W.A., Kulhawy, F.H., 2001. Contribution to piled raft foundation design. J. Geotech. Geoenviron. Eng. 127 (1), 17–24.
Rabiei, M., Choobbasti, A.J., 2016. Piled raft design strategies for high rise buildings. Geotech. Geol. Eng. 34, 75–85.
Ranjan, G., Rao, A.S.R., 2007. Basic and applied soil mechanics. New Age International.
Reul, O., 2004. Numerical study of the bearing behavior of piled rafts. Int. J. GeoMech. 4 (2), 59–68.
Reul, O., Randolph, M.F., 2004. Design strategies for piled rafts subjected to nonuniform vertical loading. J. Geotech. Geoenviron. Eng. 130, 1–13.
Sanctis, L.D., Mandolini, A., 2006. Bearing capacity of the piled rafts on soft clays. J. Geotech. Geoenviron. Eng. 132, 1600–1610.
Seo, Y.K., Choi, K.S., Jeong, S.G., 2003. Design charts of piled raft foundations on soft clay. In: Proc., the Thirteenth International Offshore and Polar Engineering Conference, Hawaii, USA, pp. 753–755.
Shrestha, S., Nadarajah, R., Parishad, R., 2017. Robust Geotechnical Design of Piled-raft Foundations for Tall Onshore Wind Turbines. Geotechnical Frontiers, pp. 204–213.
Sinha, A., Hanna, A.M., 2016. 3D Numerical model for piled raft foundation. Int. J. GeoMech. https://doi.org/10.1061/(ASCE)GM.1943-5622.0000674.
Viggiani, C., 2001. Analysis and Design of Piled Raft Foundations. First Arrigo Croce Lecture. Rivista Italiana Di Geotechnica, pp. 47–75.